Research Article

Hui Li, Neil J. Naples, Xin Zhao and Allen Y. Yi*

An integrated approach to design and fabrication of a miniature endoscope using freeform optics

DOI 10.1515/aot-2016-0031
Received May 9, 2016; accepted July 5, 2016; previously published online July 27, 2016

Abstract: Endoscopes are important medical optical devices widely used in minimally invasive surgery. However, manufacturing issues such as tight packaging constraints and tolerance requirements hinder their development. These problems often result in high manufacturing cost or poor image quality. To cope with these issues, in this research, a novel endoscope utilizing an off-axis freeform optics is developed by using an integrated ultraprecision diamond machining process. The major optical components of this endoscope include a prism with two reflective surfaces and a freeform entrance surface. In addition, a doublet and a field lens were added to complete the system design. To validate the feasibility of the endoscope design, single-point diamond turning and rastering processes were utilized to machine the required components. After the lenses were machined, the geometry of the lenses was measured using a white light optical profilometer. The results show that their profiles have a manufacture error of ±2 μm along the optical axis. Lastly, the prototype was assembled and tested to evaluate its imaging performance, including measurement of its modulation transfer function.

Keywords: diamond turning; endoscope; freeform optics; off-axis view; ultraprecision machining.

***Corresponding author: Allen Y. Yi,** Department of Integrated Systems Engineering, The Ohio State University, 210 Baker Systems Engineering, 1971 Neil Avenue, Columbus, OH 43210, USA, e-mail: yi.71@osu.edu
Hui Li, Neil J. Naples and Xin Zhao: Department of Integrated Systems Engineering, The Ohio State University, 210 Baker Systems Engineering, 1971 Neil Avenue, Columbus, OH 43210, USA

1 Introduction

Miniature endoscopes are becoming increasingly important as an optical inspection tool that expands the applicability of minimally invasive surgery. Fiber-optic endoscopes quickly have proven to be useful medical devices since their invention in 1957 [1]. Although the fiber-optic imaging endoscopic devices exhibit high flexibility in manufacturing and miniaturization, its low illumination and color-reproducing capabilities often result in poor image quality. As cleanroom technology matures, expensive optical imaging fibers have been replaced by low-cost CMOS imagers. This technological leap has improved the resolution dramatically for small-diameter endoscopes, but has come at the expense of a reduction in their field of view (FOV). Additionally, CMOS imagers need to be placed coincident with the imaging plane. This combination of tight packaging constraints and strict optical requirements presents significant challenges for manufacturing.

Recently, Wippermann et al. [2] developed a disposable low-cost video endoscope, capable of viewing both straight and oblique directions. The configuration of their endoscope consists of an aspherical polymethylmethacrylate (PMMA) lens, a BK-7 glass prism with double reflections at two angled surfaces, a gradient index rod lens (GRIN), and a spherical PMMA lens. The prism is used to tilt the optical axis of the object with respect to the mechanical axis of the packaging tube, achieving an 18° off-axis view. The GRIN lens was installed to enlarge the FOV to 110° in the straight viewing direction. In order to lower fabrication cost, they also demonstrated a diamond turning process to fabricate the two polymer lenses, which could be mass produced by molding in the future.

However, the fabrication process of Wippermann's endoscope was not readily adopted by the optical industry due to the use of the glass prism and GRIN lens. Generally speaking, glass prism fabrication requires grinding and polishing processes that will prolong the production cycles, especially when optical lenses have complicated shapes. GRIN lens fabrication, on the other hand, involves

ion-exchange and diffusion techniques in high-volume manufacturing. This diffusion process is difficult to control and only produces an approximation of a parabolic or hyperbolic secant surface [3].

Moreover, as the freeform surfaces were not included in Wippermann's original design, aberrations due to large changes in optical paths are difficult to control. In their design, had freeform optics been used, these optical aberrations would have been effectively reduced while still achieving a large depth of field and a larger FOV [4]. In terms of optical fabrication, diamond machining is an efficient method to fabricate a small number of freeform optics with high optical surface finishing. Additionally, the manufacturing process study of the endoscope helps to establish process steps for precision mold fabrication [5]. These molds can then be used in injection molding or hot embossing machines for high-volume production. These molding processes provide an alternative method by creating high-quality and low-cost optical lenses and therefore are becoming promising manufacturing methods.

In this research, we demonstrated a novel miniature endoscope by using an off-axis freeform prism based on the general idea developed by Wippermann's group [2]. As the main focus of the research, an integrated ultraprecision machining process was developed in order to establish a low-cost fabrication method for the endoscope. The endoscope in this research consists of a PMMA prism with a freeform entrance surface, two reflective surfaces, and three aspherical polymer lenses. Among these polymer lenses, a PMMA lens and a polycarbonate (PC) lens were cemented together as a doublet to reduce chromatic aberration. In this setting, this endoscope could be coupled with a color CMOS imaging sensor. All the optical components of this endoscope are made of polymers. Thus, the performance of this endoscope, such as FOV and volumetric size, may be slightly compromised as compared to endoscope systems where glass lenses are used. By using an all-polymer design, it is possible to manufacture every part of the endoscope by ultraprecision machining. In this research, a combined diamond rastering and diamond turning process were developed to fabricate both the prism and the aspherical lenses. Furthermore, the optical performance of the endoscope was tested using different optical setups.

In summary, the goal of this study was to implement an integrated ultraprecision machining process for a novel miniature endoscope using prism with a freeform optical surface. First, the design of the endoscope was analytically validated. Then, the feasibility of the fabrication process was demonstrated. Specifically, the lenses and the prism were fabricated using an integrated diamond machining process and assembled utilizing the fiducials created during the diamond machining process, and the optical performance of the endoscope was evaluated.

2 Endoscope design

As discussed earlier, the design of the miniature endoscope with a large off-axis view is a variation of an off-axis endoscope initially developed by Wippermann et al. [2]. The optical design, as shown in Figure 1, was performed using CODE V (from Synopsys Inc., Mountain View, CA, USA). The optical prescription is listed in Table 1.

In the design of this endoscope, a freeform surface having negative power was chosen as the front face of the prism to eliminate the first aspheric lens in Wippermann's design. The prescription of the freeform surface is

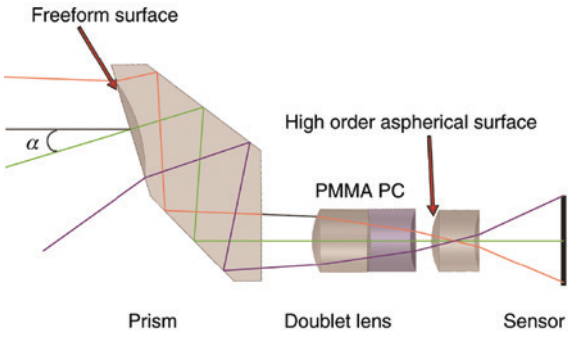

Figure 1: An off-axis endoscope design using a prism with a freeform optical surface.

Table 1: The optical prescription for the endoscope.

Surface	Radius (1/*c*)	Thickness	Material	Semiaperture (*r*)	Conic constant (*k*)
Object	–	100.000	–	–	–
1	-5.172	2.900	PMMA	2.328	-0.634
2	–	-4.500	PMMA	–	–
3	–	7.500	PMMA	–	–
4	–	2.000	–	–	–
5	2.130	1.900	PMMA	1.021	-0.170
6	-6.113	1.300	PC	0.960	13.318
7	3.027	0.500	–	0.922	5.456
8	2.276	1.500	PMMA	1.083	-4.373
9	3.030	3.500	–	1.064	-4.015
Sensor	–	–	–	1.507	-

Surface 2 and surface 3 are reflective surfaces. Units are in millimeters.

represented by a Zernike polynomial in polar coordinate as follows:

$$z=cr^2/(1+(1-(1+k)c^2r^2)^{0.5})+\sum_{i=1}^{15}A_i, \quad (1)$$

where c, r, and k are listed in Table 1; A_i values are listed in Table 2.

Unlike Wippermann's design, the optical axes of the following lenses are parallel with the mechanical axis of the packaging tube. This arrangement reduces the level of complication for assembly at the expense of volume of the optical system. Two aspherical lenses behind the prism, one made of PMMA and one made of PC, are acting as an achromatic doublet for chromatic aberration reduction. A higher-order aspherical lens surface was designed on the front face of the rear field lens to further correct spherical aberration. The design of the aspherical lens can be described as follows:

$$z=cr^2/(1+(1-(1+k)c^2r^2)^{0.5})+B_1r^4+B_2r^6+B_3r^8+B_4r^{10}+B_5r^{12}+B_6r^{14}+B_7r^{16}+B_8r^{18}+B_9r^{20}, \quad (2)$$

where c, r, and k are listed in Table 1. B_i are the higher-order coefficients, and their values are listed in Table 3. Other surfaces, namely 5, 6, 7, and 9, in the table, are represented by the equation as follows:

$$z=cr^2/(1+(1-(1+k)c^2r^2)^{0.5}). \quad (3)$$

The object distance was 100 mm, and the object heights in the X and Y directions were set at ±34 mm. The aperture of the left surface on the doublet was set as an optical stop, as shown in Figure 1. The weights of three wavelengths, 700, 550, and 400 nm, were assigned as 4:5:1, as tissue with blue color is usually not detected in medical operation. The off-axis viewing angle α is 16.7°.

A variety of analyses have been conducted in CODE V to validate the performance of the endoscope. This miniature endoscopic system has a 4.326 mm effective focal length. Its entrance pupil and exit pupil are 1.000 and 1.301 mm in diameter, respectively. The diagrams of imaging spot sizes from different object positions were plotted in Figure 2 to demonstrate the capability of the freeform surface. The left spot diagram was generated under the same optical arrangement as the right spot diagram, except that its Zernike coefficients were truncated. The root mean square spot radius of the endoscope without freeform surface would have increased from 3.8 μm to >110 μm, indicating that object could barely be imaged. Additionally, the modulation transfer function (MTF) curves, shown in Figure 3, were studied for quantitative comparison among different object positions. For each position, the MTF of the endoscope was calculated in both sagittal and tangential orientations. Fifty percent contrast at 110 LP/mm was feasible for all objective positions, and the optical system performance was only 10% less than the diffraction limit.

3 Fabrication processes

In single-point diamond turning processes, slow tool servo [6], fast tool servo [7], high-speed diamond milling [8], and rastering [9] are commonly used to fabricate freeform optical components for use in prototypes and for optical mold fabrication. Because the freeform surface on the prism has large slopes, neither slow tool servo nor fast tool servo diamond turning in a spiral cutting path can be easily applied such that collision between the clearance face of the diamond tool and the machined surface can be avoided. On

Table 2: Zernike polynomial and its coefficients for the freeform surface.

A_i	Term	Value	A_i	Term	Value	A_i	Term	Value
A_1	1	-3.639 E-2	A_6	$\rho^2\sin(2\theta)$	-3.798 E-8	A_{11}	$\rho^4\cos(4\theta)$	-1.452 E-5
A_2	$\rho\cos(\theta)$	-2.454 E-7	A_7	$\rho^3\cos(3\theta)$	-8.779 E-10	A_{12}	$(4\rho^4-3\rho^2)\cos(2\theta)$	-1.789 E-8
A_3	$\rho\sin(\theta)$	8.705 E-3	A_8	$(3\rho^3-2\rho)\cos(\theta)$	1.560 E-10	A_{13}	$6\rho^4-6\rho^2+1$	-6.399 E-6
A_4	$\rho^2\cos(2\theta)$	3.400 E-6	A_9	$(3\rho^3-2\rho)\sin(\theta)$	2.680 E-5	A_{14}	$(4\rho^4-3\rho^2)\sin(2\theta)$	1.139 E-9
A_5	$2\rho^2-1$	1.309 E-2	A_{10}	$\rho^3\sin(3\theta)$	-5.023 E-6	A_{15}	$\rho^4\sin(4\theta)$	-8.661 E-10

Table 3: Higher-order coefficients for aspherical surface.

B_i	Value	B_i	Value	B_i	Value	B_i	Value	B_i	Value
B_1	2.271 E-2	B_3	-5.201 E-2	B_5	-3.518 E-2	B_7	-1.341 E-3	B_9	-8.130 E-5
B_2	2.657 E-2	B_4	5.685 E-2	B_6	1.237 E-2	B_8	-1.734 E-4		

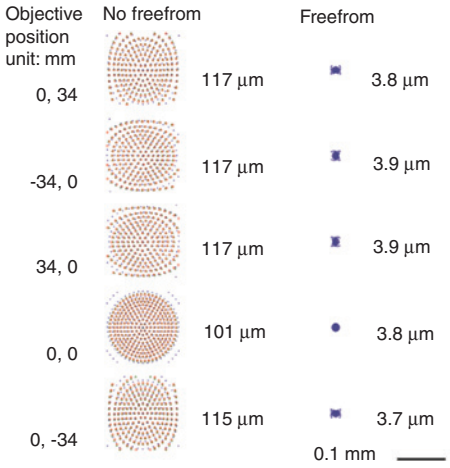

Figure 2: Comparison of imaging spot size between optical designs using aspherical surfaces and a freeform surface.

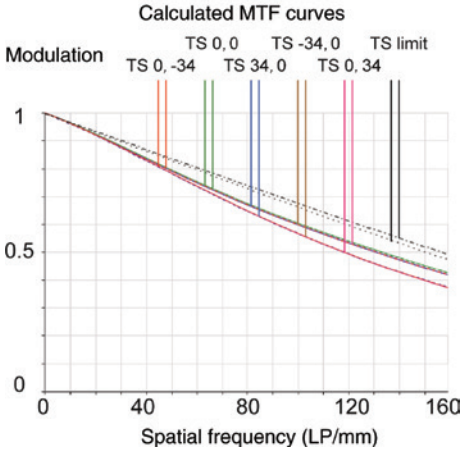

Figure 3: Computational MTF in tangential direction and sagittal direction.

the other hand, high-speed milling will require a separate setting up and therefore will interrupt the continuation of the machining process. Based on these considerations, rastering was selected to ensure that a single, non-interrupted machining process was used for fabrication.

In addition to the freeform optical surface, every other lens in the endoscope was machined on the 350 FG (Freeform Generator from Moore Nanotechnology Inc., Keene, NH, USA) as well. This process could be further developed for mold fabrication for low-cost, high-volume, and high-precision optical components.

3.1 Diamond turning process for lenses

All three following aspherical lenses were machined on larger-size PMMA or PC discs for easy handling during fabrication. Specifically, the diamond-turned outside diameter surfaces of the discs were used as the datum surfaces for both fabrication and assembly. The thicknesses of three finished discs are 3.900, 1.568, and 1.924 mm. The thicknesses of these lenses were designed such that the need for spacers between the lenses is eliminated. Thus, the final thickness of each lens is the sum of the distance between adjacent surfaces of two lenses and the thickness of the original design. Once the three lenses were machined, they were assembled by simply stacking face to face as shown in Figure 4. No translational alignment in the axial direction is needed for the optical test because all three lenses are circular in shape with identical diameters. Lens 1 and lens 3 were turned by a diamond tool with 2.606 mm tool nose radius, while lens 2 was turned by a smaller diamond tool with 0.379 mm tool nose radius. The nose radii of the diamond tool were compensated offline in the calculation for tool path trajectory. The rough cutting feed rate and cutting depth were 20 mm/min and 10 μm. The finishing cut feed rate and cutting depth were 2 mm/min and 2 μm.

The PMMA and PC discs were first rough machined on a common lathe. Extra stock of 100 μm for the finishing process was left in both axial (for disc thickness) and radial directions for all the discs (for outside diameter). The disc was then waxed on an aluminum mandrel that was already diamond machined on both ends. The outside diameter surface and the flat surface were turned using the same diamond tool with a sweep angle of >90°. This process ensures the perpendicularity between the circumferential surface and the flat surface – a critical step for optical assembly. Afterwards, the disc was flipped to be vacuum chucked to machine the opposite surface. It was centered around the spindle axis within 1-μm accuracy by indicating on the circumferential surface. A rough and a finishing diamond turning process were subsequently performed for the first side of the lens surface after facing the flat. Finally, the disc was flipped again and vacuum chucked. The other side of the lens surface was also diamond turned by similar rough and finishing processes.

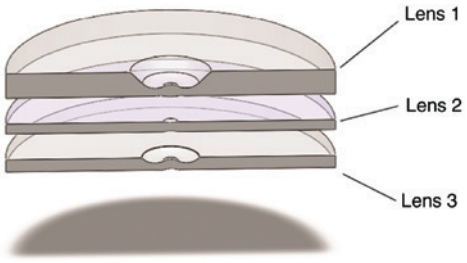

Figure 4: Assembly of the three aspherical lenses.

3.2 Diamond rastering process for prism

It would be extremely challenging to grind and polish the prism as it contains both a freeform and two reflective flat surfaces. The angles and distances between each two surfaces are crucial parameters for the prism. In contrast to the conventional lens manufacturing process, diamond machining is much more capable of fabricating optics with complex three-dimensional profiles, which could be further developed for microprecision injection molds or compression molds. Although ultraprecision diamond machining is a capable and versatile process, there are some issues associated with this process, especially when slow tool servo or rastering are used. One of the issues is the higher magnitude of the residual tool marks [10] compared with grinding. By optimizing the machining conditions and parameters, the effects of the residual tool marks can be minimized.

In order to shorten the rastering process and therefore minimize the environmental influence such as temperature variation and floor vibration, the prism was first roughed out on a Haas VF3 (from Haas Automation Inc., Oxnard, CA, USA) vertical milling machine. This blank was roughed out with material on all sides with an extra stock of 300 µm, to be subsequently diamond machined. Additionally, the rough prism-shape boss was machined on a tapered base, which was then firmly mounted on the 350 FG. A square shoulder was machined into the tapered surface of the blank and is parallel with the first rastered surface of the prism. This was used for orientation of the diamond tools at the beginning of the rastering process.

The rough prism was mounted on the vacuum chuck of the 350 FG as shown in Figure 5A. The diamond tool with a tool nose radius of 400 µm and 0° rake angle was installed in the *X* axis (horizontal direction). The feed of the tool moves upward in the *Y* direction while horizontally stepping along the *Z* direction. The tool path was compensated based on the freeform surface profile and the diamond tool nose radius. During rastering, the spindle on the machine (*C* axis) was held in a constant position. After the rastering of each face of the prism was completed, the spindle was rotated sequentially according to the angle between two adjacent surfaces on the prism. The rastering feed rate for the flat surfaces was set at 500 mm/min. For rough rastering, the cutting depth was 10 µm and the cross-feed step along the *Z* axis was 40 µm. For finishing rastering, the cutting depth was 2 µm and the cross-feed step along the *Z* axis was 10 µm.

The entire process consists of the aforementioned rough machining and freeform surface machining by rastering. The maximum slope of the concave freeform surface on the prism is 28.8°, which means a tool with a clearance angle of <28.8° would interfere with the freeform surface during the rastering process. To cope with this issue, the face where the freeform surface was to be rastered was tilted -20° along the *Z* axis such that it could be machined with a tool of 10° clearance angle, as shown in Figure 5B. Figure 6 shows the color map and the contour lines of the tilted freeform surface.

4 Evaluation of the miniature endoscope

4.1 Geometry measurement of the lens surface

The geometry measurement was performed on a white light noncontact interferometer-based optical profilometer (Wyko NT9100, Veeco Instruments Inc., Plainview, NY, USA). Surface 6 in Table 1 was chosen for its mild curvature such that more light could be reflected into objective lens of Wyko under the same condition compared with the

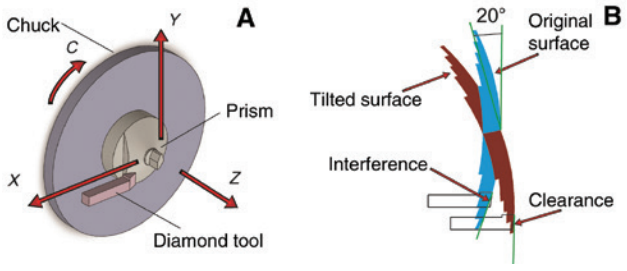

Figure 5: (A) Diamond rastering setup for the prism. (B) Interference problem can be resolved by tilting the freeform optical surface.

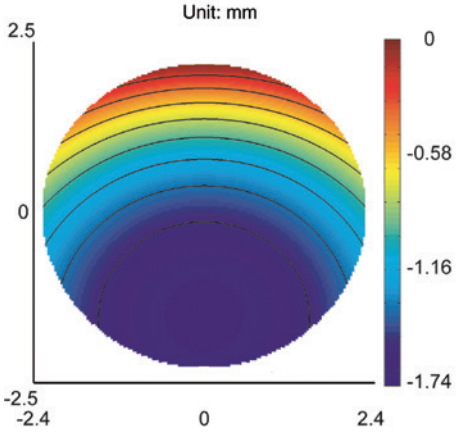

Figure 6: Color map and contour line of the tilted freeform surface on the prism.

other surfaces. Therefore, it is less likely to lose information during scanning. For the measurement, the magnification was set at 27.4× and the stitching function was used to obtain a high-resolution scan of the entire lens surface. The tilt of the scanned surface was automatically removed. The complete profile of surface 6 is shown in Figure 7A. A cross-section profile was drawn in Figure 7B. The solid line and the dashed line represent the design surface profile and the measured surface profile. According to the corresponding deviations between the two surface profiles plotted in Figure 7B, the absolute deviation was within ±2 µm.

4.2 Imaging performance

The optical performance of the off-axis endoscope was tested on a home-built setup. A CCD camera (PL-B957F, PixeLINK Inc., Ottawa, Ontario, Canada, 8.98 mm by 6.70 mm) with a 6.45 µm pixel pitch was employed. A zoom lens (VZMTM 450i; Edmund Optics Inc., Barrington, NJ, USA) with magnification ranging from 0.75× to 4.5× was mounted onto the camera to observe the images through the endoscope. A United States Air Force (USAF) test target was used to evaluate the imaging performance of this endoscope, as in Figure 8. To measure the FOV, an aluminum block (24 mm by 24 mm) was used as a target in the following imaging test. When it was around 90 mm away, the block was circumscribed by the aperture of the endoscope. Thus, the half angle of the FOV of this endoscope is 10.7° according to

$$\text{half of FOV} = \arctan\left(\frac{24\times\sqrt{2}}{90\times 2}\right)\times\frac{180}{\pi}.$$

4.3 MTF measurement and tolerance analysis

The MTF of the entire lens assembly was measured to evaluate the optical performance of the endoscope. In this experiment, a slanted edge target test was performed. A snapshot of a checker board with 5° rotation was collected and calculated in Quick MTF (www.quickmtf.com), an image quality test program. In this program, the combination of centroid calculation and hamming window was selected to minimize edge detection error. In addition, in the measurement, the linear regression was turned off for geometric distortions of the slanted edge. The experimental MTF results are depicted in Figure 9. The contrast falls to 15% around 30–40 LP/mm

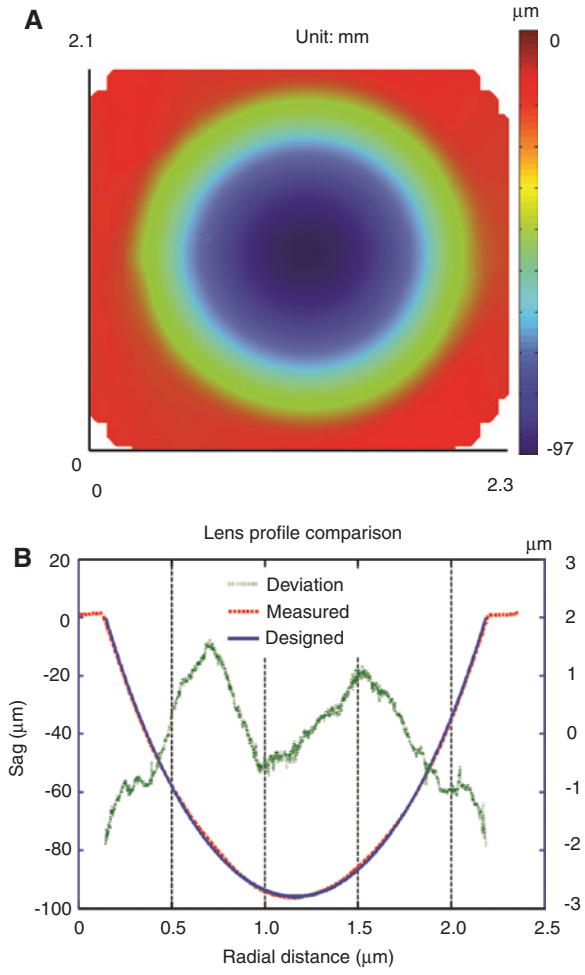

Figure 7: (A) Measured surface 6 using Wyko profilometer. (B) Cross-section profiles of the design and measured surface 6 and its deviation.

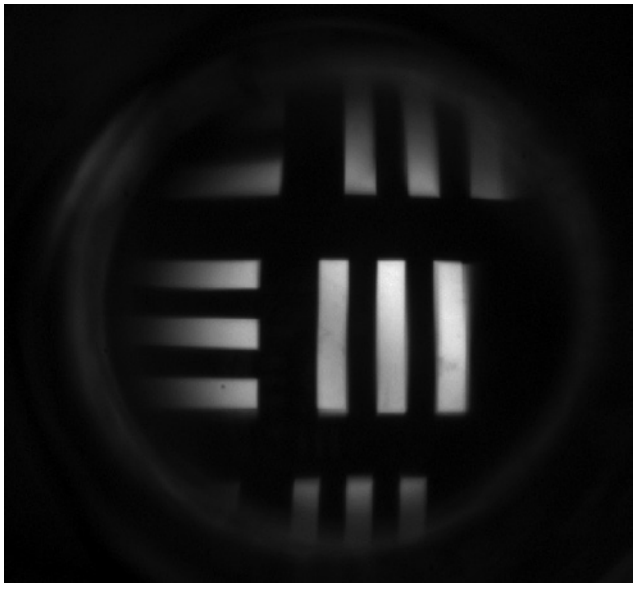

Figure 8: Imaging test of the endoscope.

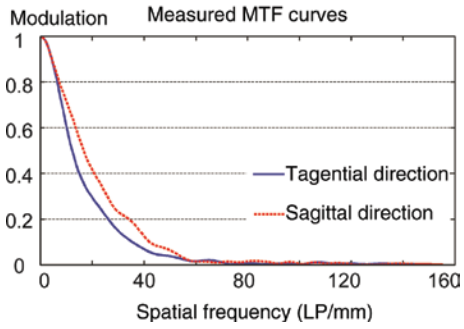

Figure 9: MTF in tangential and sagittal directions.

in both tangential and sagittal directions. Although the experimental results show that the real endoscope system has lower resolution than the plot from the original design in Figure 3, this result is still considered to be acceptable given that the Nyquist frequency of the test camera is 77.5 LP/mm. The causes of less than design MTF value may include several possible sources: low and/or non-uniform illumination, residual tool marks, other fabrication errors, and misalignments of optical components.

To evaluate if the aforementioned errors occurred in fabrication, tolerance analysis is performed at 30 LP/mm in CODE V. Tolerance of the optical component fabrication and alignment are specified in Table 4. According to the surface form accuracy, surface irregularity was set as four fringes assuming the wavelength of test light at 500 nm. Other tolerance values are based on common fabrication experience [11]. From Figure 10, MTF in the sagittal direction drops less than that in the tangential direction, which is also consistent with the experiment results.

Table 4: Tolerance value of the endoscope.

Tolerance item	Value
Thickness (mm)	±0.01
Surface irreg. oriented 0° and 45°	Four fringes
Surface decenter x and y (mm)	±0.01
Surface tilt α and β (radian)	±0.000145

5 Discussion and conclusions

The refractive indices of optical polymers are slightly lower in comparison with most optical glasses. Therefore, the PMMA prism has less power to steer light than its glass counterparts. The diameter of this endoscope will be slightly larger than 3 mm as compared to Wippermann's design, from which our optical design was originated. The usage of a GRIN lens also drastically converged the light rays in Wippermann's design, which was important for reducing the overall length of the endoscope. In Wippermann's design, the optical axis was also bent after leaving the prism. This results in a more compact structure and a larger off-axis angle, but creates a lot of difficulties for testing and assembly.

In this research, a freeform surface was designed and integrated with the prism. The freeform optical surface helps to shrink the imaging spot from >110 μm if only aspherical lenses were used to <4 μm, and therefore improves the overall resolution of the endoscope. According to its MTF, this endoscope is only around 5% below the diffraction limit at half-Nyquist spatial frequency of the imaging sensor and therefore is more than sufficient to avoid aliasing effects.

An integrated diamond machining process was developed to fabricate a prototype of the endoscope for optical test. In this research, the absolute deviation was discovered to be almost symmetric along the optical axis of the lens, a result of the diamond turning process used. In addition to the random environmental factors such as temperature variations, vibration, structural deflection of the ultraprecision

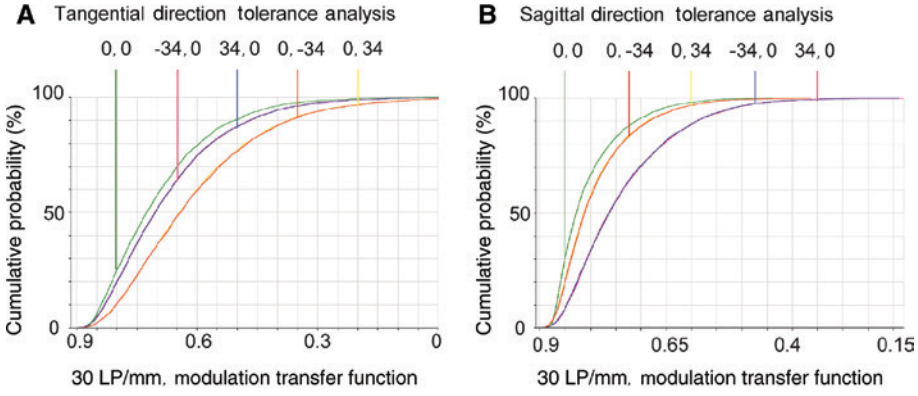

Figure 10: Cumulative possibility tolerance analysis: (A) tangential direction, (B) sagittal direction.

machine due to its weight, and uneven heating, machining process variations, such as following error of tool position, also affect the finish quality of the optical components. Moreover, to achieve a larger clearance angle during the rastering of the freeform entrance surface on the prism, the rough prism was tilted -20° along the *Z* axis. Therefore, the diamond tool machined the large part of the freeform surface with a very large negative rake angle, resulting in a slightly higher surface roughness value.

In addition to the aforementioned errors in fabrication, the misalignment of the optical components always results in performance loss. In this endoscopic configuration, during testing, the freeform-based prism was mounted on a fixture while three lenses were concentrically aligned to each other and mounted on a separate multi-degree of freedom stage. Any misalignment from the optimal position between the prism and the following lenses could have affected the imaging. In this assembly, wedge, de-centration of the lenses, tilt of the lenses in assembly, and position variance along the optical axis could all have introduced errors during the testing.

Optical aberrations are another source of errors during the imaging test of this endoscope. For example, chromatic aberration still existed although a doublet was installed in the assembly, resulting in blurs in the image and thus bringing degradation in MTF. Moreover, the separation between sagittal and tangential MTF was also partially caused by lateral chromatic aberration as in Figure 9.

In summary, a novel freeform optical surface-based off-axis miniature endoscope was designed and computationally validated in CODE V. The endoscope consists of a prism with a freeform optical surface and three following aspherical lenses assembled using simple fiducial features. An integrated ultraprecision machine process was developed to fabricate all the optical components of the endoscope. Geometric measurements were acquired for a selected lens surface to evaluate the reliability of the ultraprecision machining process. A prototype was built and tested for imaging performance and more specifically the modulation transfer function was evaluated. To achieve even lower manufacturing cost, future work would include mold fabrication using ultraprecision machining and subsequently wafer-level molding process for high-volume production.

Acknowledgments: This study was partially based on the work supported by National Science Foundation, Division of Industrial Innovation and Partnerships, under grant number 1448935. Any opinions, findings, and conclusions or recommendations expressed in this material are those of the authors and do not necessarily reflect the views of the National Science Foundation.

References

[1] J. M. Edmonson, Gastrointest. Endosc. 37, S27 (1991).
[2] F. C. Wippermann, E. Beckert, P. Dannberg, B. Messerschmidt and G. Seyffert, P. Soc. Photo-opt. Ins. 7556, 755607 (2010).
[3] S. Sinzinger, J. Jahns, in 'Microoptics' (Wiley-VCH, Weinheim, Germany, 1999) pp. 118–119.
[4] F. Z. Fang, X. D. Zhang, A. Weckenmann, G. X. Zhang and C. Evans, CIRP Ann. Manuf. Techn. 62, 823 (2013).
[5] P. He, F. Wang, L. Li, K. Georgiadis, O. Dambon, F. Klocke, et al., J. Opt. 13, 085703 (2011).
[6] A. Y. Yi and L. Li, Opt. Lett. 30, 1707 (2005).
[7] W. Gao, T. Araki, S. Kiyono, Y. Okazaki and M. Yamanaka, Precis. Eng. 27, 289 (2003).
[8] S. Scheiding, A. Y. Yi, A. Gebhardt, R. Loose, L. Li, et al., Proc. SPIE 7927, 79270N (2011).
[9] L. Li and A. Y. Yi, J. Opt. Soc. Am. A 27, 2613 (2010).
[10] L. Li, S. A. Collins Jr., and A. Y. Yi, J. Manuf. Sci. Eng. 132, 021002 (2010).
[11] Y. Zou, W. Zhang, F. S. Chau and G. Zhou, Opt. Express 23, 20582 (2015).